RESEARCH ARTICLE

Catalytic activity, selectivity, and stability of co-precipitation synthesized Mn-Ce mixed oxides for the oxidation of 1,2-dichlorobenzene

Juan Qiu[1] · Yaqi Peng[1] · Minghui Tang[1] · Shengyong Lu[1] · Xiaodong Li[1] · Jianhua Yan[1]

Abstract

Mn-Ce mixed oxides were prepared using a simple, facile, and high yielding co-precipitation method. The effects of the proportion of Mn/Ce and the addition of Fe, Co, Sn on the physical and chemical properties of catalysts have been thoroughly investigated. Several analytical techniques were conducted, namely BET, XRD, SEM, XPS, and H_2-TPR. Compared with other catalysts, MCFe shows the highest specific surface area of 108.2 m^2/g and Dp of 7.2 nm. The XRD results indicated that the diffraction peaks were dominated by Mn_2O_3, the pyrolusite MnO_2, and hausmannite Mn_3O_4. SEM observations showed nano-particle and plate-like structures. XPS analysis indicated that there is electron exchange between both Mn^{3+} and Mn^{4+} as well as Ce^{3+} and Ce^{4+} which promotes catalytic oxidation. The H_2-TPR profiles displayed two dominant peaks located around 250 °C and 310 °C. Catalytic activity, selectivity, and stability of co-precipitation synthesized Mn-Ce mixed oxides for the oxidation of 1,2-dichlorobenzene were tested. The selectivity of MCFe towards CO_2 and CO reached 96 % at 270 °C. At 180 °C, MCFe had the optimum stability with a removal efficiency of about 50 %. At last, the main byproducts were identified by GC-MS. Possible reaction paths were proposed. The Mn-Ce mixed oxides catalysts may be a more economical alternative for industrial application.

Keywords 1,2-Dichlorobenzene · Co-precipitation · Mn-Ce mixed oxides · Catalytic oxidation · Products analysis

Introduction

The incineration of waste such as municipal and medical waste emits polychlorinated dibenzo-p-dioxins and dibenzo-furans (PCDD/Fs), which were persistent in the environment and could bioaccumulate in living organisms (Ssebugere et al. 2019). 1,2-Dichlorobenzene was often chosen as model compound of PCDD/Fs, to evaluate the activity of the catalyst in the oxidation of an aromatic ring, as well as its resistance to chlorine poisoning (Debecker et al. 2007). Recently, CVOC

Juan Qiu and Yaqi Peng contributed equally to this work.

Responsible Editor: Santiago V. Luis

✉ Shengyong Lu
  lushy@zju.edu.cn

✉ Jianhua Yan
  yanjh@zju.edu.cn

[1] State Key Laboratory for Clean Energy Utilization, Institute for Thermal Power Engineering, Zhejiang University, Hangzhou 310027, China

emissions are being controlled by various abatement technologies such as adsorption, thermal, and catalytic oxidation. Catalytic oxidation is operated at relatively low temperatures and has been confirmed to be an efficient and economical method that can meet strict emission standards (Liu et al. 2021). Numerous types of noble metal, ceria and mixed transition metal oxide catalysts have been referenced in literatures (Zhao et al. 2020a, b; Deng et al. 2020). Among the transition metal oxides, Mn and Ce oxides are regarded as effective catalysts with high oxygen storage capacity as well as oxygen mobility at low temperatures (Long et al. 2019). In recent studies, Mn-CeOx prepared by a variety of methods has been reported in the catalytic removal of VOCs (Yang et al. 2020). Wang et al. discovered that MnOx (0.86)-CeO₂ catalysts made by the sol-gel method displayed high stability in the oxidation of chlorobenzene (CB) (Wang et al. 2009). A study by Zhang et al. conveyed that the Mn-CeOx catalysts which were hydrothermally synthesized exhibited higher catalytic activity of toluene (Zhang et al. 2020).

Researchers have become increasingly interested in catalysts prepared by co-precipitation; therefore Sun et al. investigated rare earth metal doped Mn catalysts that improved the oxidation

efficiency, and the NO conversion for the Mn-Ce-Ox catalyst exceeded 90% (Sun et al. 2018). Tang et al. also found out that the MnOx-CeO$_2$ catalyst exhibited greater catalytic activity for the oxidation of HCHO and 1,2-dichlorobenzene (1,2-DCB) when prepared by the co-precipitation method (Tang et al. 2006; Martín-Martín et al. 2020). Furthermore, the effect of the Ce to Mn mole ratio as well as the calcination temperature on carbon monoxide oxidation at lower temperatures has been studied (Venkataswamy et al. 2015). Chen et al. conveyed that the 3Mn1Ce synthesized by hydrolysis demonstrated good oxidation performance for VOCs (benzene, o-xylene, and chlorobenzene) (Chen et al. 2018). Lin et al. reported that Mn^{4+}/Mn^{3+} and Ce^{4+}/Ce^{3+} might have played important roles in catalytic oxidation due to the increase in oxygen vacancies in MnOx-CeO$_2$ (Lin et al. 2018).

During the catalytic oxidation of CVOCs, the catalysts are prone to deactivation by chlorine contained in the 1,2-DCB or other byproducts, and the oxidation of 1,2-DCB leads to secondary pollution (Chen et al. 2018). Lin et al. summarized the final products and multiple byproducts distributed in effluent gas, discovering that CO was dominant at low temperatures and CO$_2$ was dominant at higher temperatures. HCl could be detected and Cl$_2$ could hardly be detected at low temperatures (Lin et al. 2021). Zhao et al. reported on the distribution of products in DCM and CB oxidation, determining that CHCl$_3$ was formed and that chlorination cannot occur without the oxygen species (Zhao et al. 2020a). Sun et al. reported that the loading of alkali potassium could enhance the HCl/CO$_2$ selectivity and inhibit catalytic oxidation of chloroaromatics (Sun et al. 2016a).

Co-precipitation is a simple, economical and high yielding method in industrial application (Shao et al. 2019); therefore we herein report a series of Mn and Ce oxide catalysts and Fe, Co, Sn doped Mn-Ce oxide catalysts via co-precipitation. Catalytic activity, selectivity and stability of co-precipitation synthesized Mn-Ce mixed oxides for the oxidation of 1,2-dichlorobenzene were evaluated, and then the catalysts were characterized by different methods. The byproducts in the 1,2-DCB oxidation process were analyzed, and possible reaction paths were proposed.

Materials and methods

Catalyst preparation

The Mn and Ce oxide catalysts were prepared by the co-precipitation method. 0.55 mol/L Mn(NO$_3$)$_2$ and 0.35 mol/L Ce(NO$_3$)$_2$ and 0.35 mol/L Fe(NO$_3$)$_2$, Co(NO$_3$)$_2$, SnCl$_2$ were prepared and acted as precursors. Each precursor was dissolved separately, then the two precursors were mixed together and stirred at mild conditions. A NH$_2$COONH$_4$ solution was added dropwise into the mixed solution until the pH value reached 9 and precipitation was formed. The obtained

precipitate was kept at room temperature for 2 h, then filtered and washed repeatedly with distilled water. The solid matter was dried at 110 °C for 12 h and calcined at 500 °C for 3 h. Six catalysts with different components and ratios were prepared by this procedure, namely MC-1 (1Mn0Ce) (pure MnO$_x$), MC-2 (8Mn2Ce), MC-3 (7Mn3Ce), MC-4 (5Mn5Ce), MC-5 (3Mn7Ce), MC-6 (0Mn1Ce) (pure CeO$_x$), MCFe (8Mn2Ce2Fe), MCCo (8Mn2Ce2Co), and MCSn (8Mn2Ce2Fe).

Characterizations

N$_2$ adsorption/desorption curves were measured by Micromeritics TriStar 3020, and the specific surface area and average pore size were calculated by the Brunauer-Emmett-Teller (BET) model. The total pore volume was obtained by a Barrett-Joyner-Halenda (BJH). The micromorphology of catalysts was analyzed by a SU-8010 scanning electron microscope (SEM). The XRD patterns of the samples were attained by a Philips Model XD-98 X-ray diffractometer (XRD) with Cu K$_\alpha$ radiation (λ = 0.15406 nm) and a scanning rate of 0.02 °/min. The X-ray photoelectron spectroscopy (XPS) of the samples were analyzed by an ESCALab 250Xi with Al Kα X-rays. The binding energy value was set to C 284.5 eV. H$_2$ temperature programmed reduction (H$_2$-TPR) was carried out by a chemical adsorption analyzer (Micromeritics Autochem II 2920). Prior to the H$_2$-TPR experiment, 100 mg of the sample was pretreated in He gas at a flowrate of 50 ml/min at 500°C for 1 h and cooled to 50°C, and then the sample was cleaned with H$_2$/Ar gas at a flowrate of 50 ml/min. The sample was subsequently heated from 50 to 700 °C at a heating rate of 10°C/min. The H$_2$ consumption was recorded by a thermal conductivity detector (TCD).

Activity measurements

Catalytic activity, selectivity, and stability of Mn-Ce mixed oxides for the oxidation of 1,2-dichlorobenzene were evaluated in a tubular quartz reactor at atmospheric pressure. The temperature of the reactor was controlled with an electric furnace and was raised stepwise from 120 to 360 °C. 1,2-DCB was generated by the bubbling method, and the initial concentration of the 1,2-DCB was 108 ppm. The volume flow was controlled at 200 ml/min by mass controllers with 10 vol.% O$_2$ and N$_2$ as the balance gas. The gas hourly space velocity was set as 12000 h^{-1}.

Residual 1,2-DCB in the effluent gas was analyzed by a gas chromatograph (FULI) equipped with a 30-m column (DB-5) and a flame ionization detector (FID). The removal efficiency (RE) for 1,2-DCB was calculated by Eq. (1)

$$RE(\%) = \frac{[1,2-DCB]_{inlet} - [1,2-DCB]_{outlet}}{[1,2-DCB]_{inlet}} * 100 \qquad (1)$$

The yields of CO, CO_2, are calculated by Eqs. (2) and (3), respectively:

$$Y_{CO}(\%) = \frac{[CO]_{outlet}}{6[1,2-DCB]_{inlet}} * 100 \qquad (2)$$

$$Y_{CO_2}(\%) = \frac{[CO_2]_{outlet}}{6[1,2-DCB]_{inlet}} * 100 \qquad (3)$$

$$Y_{CO+CO_2}(\%) = \frac{[CO+CO_2]_{outlet}}{6[1,2-DCB]_{inlet}} * 100 \qquad (4)$$

The concentration of CO_2/CO, HCl and CH_4, $C_3H_6O_2$, C_6H_5Cl, CH_4O, C_2HCl_3, CH_2O_2 in the effluent gas was analyzed using a DX4000 Gasmet FT-IR gas analyzer. The intermediate products were identified by a gas chromatography and mass spectrometry (GC/MS) analyzer (an Agilent 7890A gas chromatograph and an Agilent 5975C mass spectrometer). The off-gases were first captured with a Tenax-GR for 30 min and then released into a thermal desorption instrument (PERSEE-TP7, China) connected to a GC/MS analyzer.

Results and discussion

BET analysis

Table 1 lists the specific surface area (S_{BET}), the total pore volume (V_p), and average pore diameter (D_p) of the catalysts and reference samples which were prepared by the co-precipitation method. The pure MnO_x catalyst (MC-1) shows a relatively lower specific surface area of 21.1 m^2/g and pore volume of 0.26 cm^3/g. After doping with Ce, its specific surface area value and pore volume evidently increased, which is helpful to the adsorption of 1,2-DCB. The D_p decreased from 24.7 to 10.3 nm. After the addition of Fe, Co, Sn, its specific surface area value increased and D_p decreased; MCFe shows the highest specific surface area of 108.2 m^2/g and D_p of 7.2 nm. In comparison to the reference samples, the catalysts prepared in this work shows larger surface area and pore volume, but smaller average pore diameter.

XRD analysis

The XRD patterns for all catalysts in the range of 10–80° were shown in Fig 1. For the MC-1 catalyst, the corresponding diffraction peaks show the main phase of crystallinity Mn_2O_3 (PDF#73-1826), the pyrolusite MnO_2 (PDF#72-1984), and the weak diffraction peaks of the hausmannite Mn_3O_4 (PDF#80-0382). It could be observed that the samples of MC-1 displayed the main distinct diffraction peaks at ca. 17.9°, 23.1°, 28.9°, 32.9°, 36.1°, which belonged to (101), (121), (110), (222), and (211) characteristic lattice plane of MnO_x, respectively. The main lattice planes were (222) and (211) where Mn_2O_3 and Mn_3O_4 were correspondingly located. For the MC-6 catalyst, characteristic diffraction peaks corresponded to CeO_2 (PDF#78-0694). There were four distinct diffraction peaks at 28.5°, 33.0°, 47.5°, 56.3° which belonged to (111), (200), (220), (311) characteristic lattice plane of CeO_2, respectively. The main lattice plane was CeO_2 located at (111) (Chen et al. 2018). Following the incorporation of Ce, the diffraction peak assigned to the MnO_2 increased in intensity and resulted in a shift of the diffraction peak of Mn_2O_3 towards a lower angle. Further increase in the Ce/Mn ratio increased the intensity in the peak corresponding to CeO_2. However, the emergence of weak Mn_3O_4 peaks can be ascribed to the Mn species segregated from the Ce lattice. After the addition of Fe, Co, Sn, the main crystalline phases are MnO_2 and Mn_3O_4 (Wang et al. 2018), which contribute to the catalytic oxidation of 1,2-DCB.

SEM analysis

The SEM images were adopted to analyze the micro structure of catalysts. Figure 2 shows the SEM images of all the samples, respectively. MC-1 and MC-2 exhibited similar nanoparticle structures. Adding Ce decreases the particle size of Mn. MC-3 and MC-4 contain nanoparticles and plate-like structures, whereas MC-5 and MC-6 samples mainly contained plate-like structures. The nanoparticles in MC-1, MC-2 samples show a porous structure, which was favored for 1,2-DCB adsorption. After doping with Ce, the surface of the samples seemed compact, which was favorable for introducing extra active sites for catalytic oxidation. After the addition of Fe, Co, Sn, MCFe, MCCo, MCSn mainly contains nanoparticles and has a porous structure which is conducive to the loading of active components on the surface.

Table 1 Pore structural data of the different samples

Sample	S_{BET} (m^2/g)	V_p (cm^3/g)	D_p (nm)
MC-1	21.1	0.26	24.7
MC-2	62.5	0.32	10.3
MC-3	67.6	0.36	10.8
MC-4	65.2	0.45	13.8
MC-5	83.5	0.46	11.1
MC-6	60.9	0.54	17.7
MCFe	108.2	0.39	7.2
MCCo	80.3	0.29	7.3
MCSn	73.3	0.38	10.3
Ref-$Mn_1Ce_1O_x$ (Deng et al. 2018)	50.2	0.12	10.2
Ref-$Mn_1Ce_2O_x$ (Shao et al. 2019)	73.3	0.10	9.8

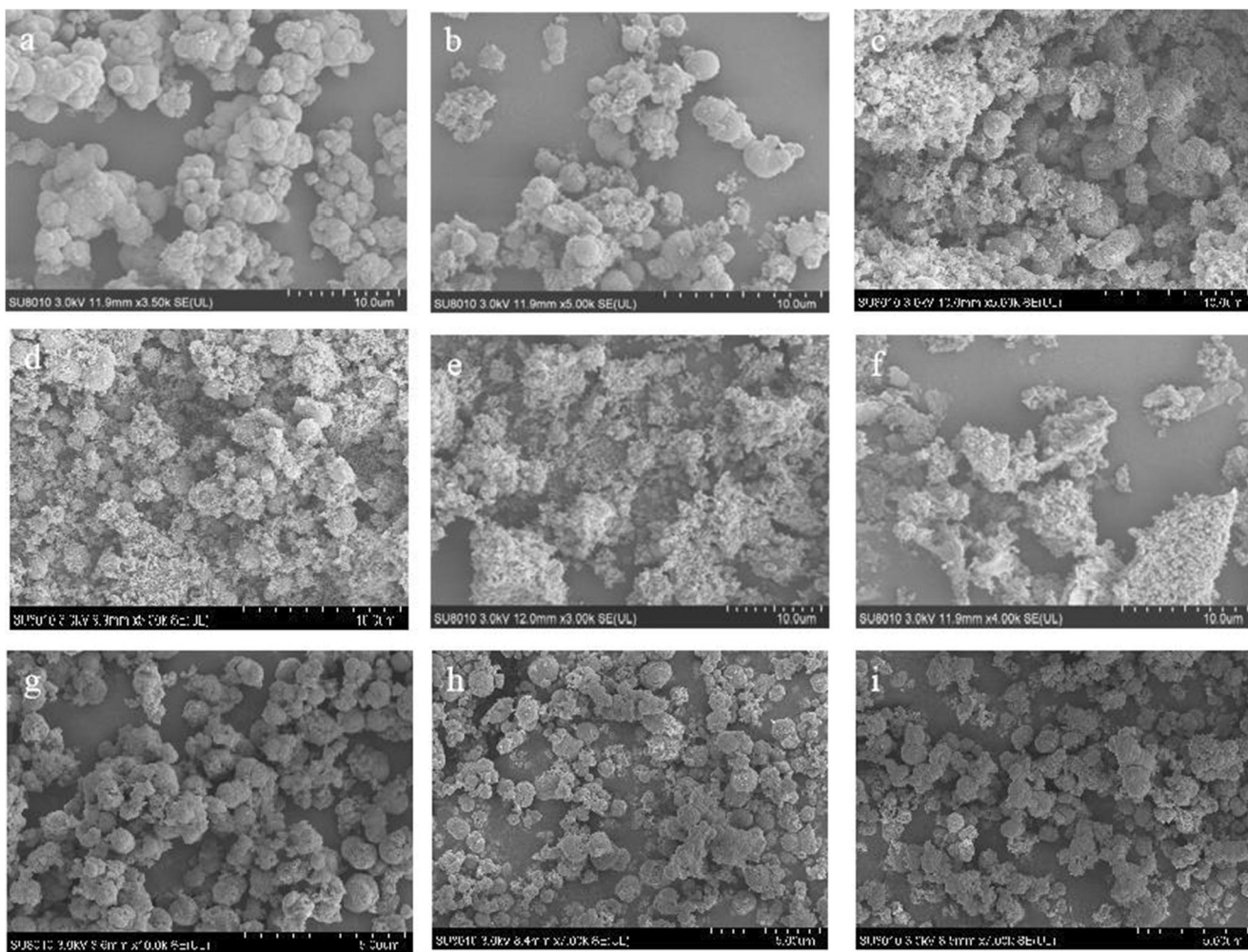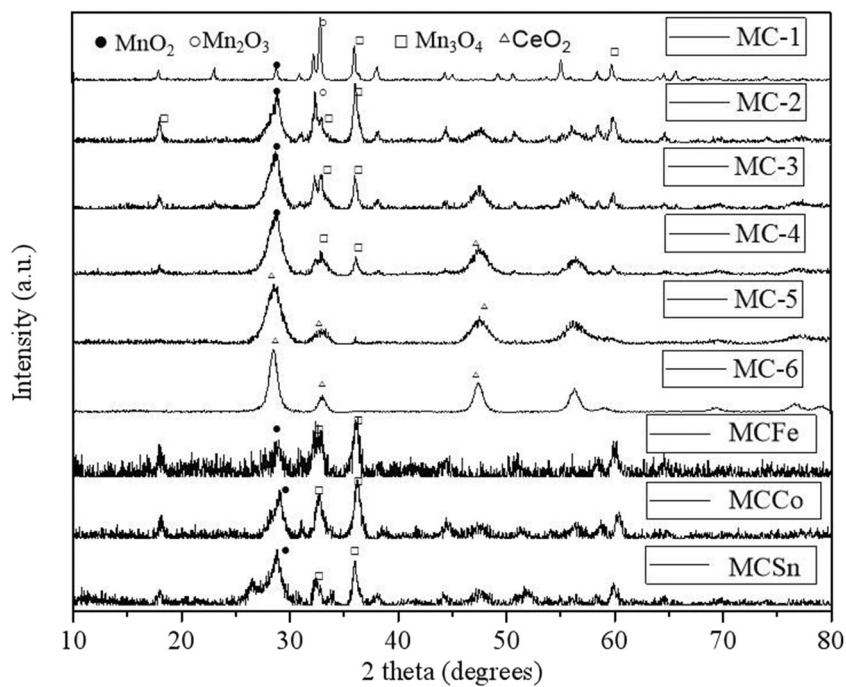**Fig. 1.** XRD patterns of the Mn-Ce catalysts

Fig. 2. SEM images of Mn-Ce catalysts. **a** MC-1, **b** MC-2, **c** MC-3, **d** MC-4, **e** MC-5, **f** MC-6, **g** MCFe, **h** MCCo, **i** MCSn

XPS analysis

XPS was applied to characterize the oxidation states of the elements and oxygen species on the catalyst surfaces. The survey spectrum of the samples and chemical states of elements were presented in Fig. 3 and Table 2, respectively. The binding energies of the Mn 2p $_{3/2}$ peaks were located at 641.0-642.0 eV and 642.0–643.0 eV, assigned to Mn^{3+} and Mn^{4+}, respectively (Liu et al. 2021). Compared with pure MnOx, the peak of Mn^{3+} and the peak of Mn^{4+} slightly shift toward higher binding energies after Ce modification, from 641.6 to 642.1 eV and from 643.5 to 644.5 eV, respectively. This deviation in the XPS means that the electron cloud densities of Mn^{3+} and Mn^{4+} were enhanced (Liu et al. 2021). Simultaneously, the concentration of Mn^{4+} increased from 54.06% (MC-5) to 72.54 % (MC-3). Compared with MC-2, after the addition of Fe, Co, Sn, the binding energy of Mn^{4+} shifted to the lower position of 1.1 eV, 1.7 eV, and 1.9 eV. This indicates that new complex substances, mainly FeMn, CoMn, and SnMn, were produced. The amount of Mn^{4+} in MCFe increased to 60.14 %, and the higher valence state of Mn benefits the formation of oxygen vacancies.

The Ce spectra of catalysts (Fig. 3B) were decomposed into Ce $3d_{5/2}$ and Ce $3d_{3/2}$, respectively. The two peaks at around 882.5 eV, 890.0 eV, 897.5 eV and 900.5 eV, 908.5 eV, 917.3 eV could be assigned to Ce^{4+} 3d, and the other peaks 885.0 eV and 903.2 eV were ascribed to the surface Ce^{3+} 3d (Zhao et al. 2020b). The percentage of Ce^{3+}/Ce^{4+} was listed in Table 22. After combining with Mn, the relative percentage of Ce^{4+} increased from 54.6 to 70.82 %; the higher relative content of Ce^{4+} means a higher content of oxygen vacancies of the catalyst. After the addition of Fe, Co, Sn, the amount of Ce^{4+} in MCFe, MCCo, MCSn increased to 73.07 %, 78.43 %, and 77.72 %, respectively.

The O1s spectra of the catalysts are presented in Fig. 3C. There were several distinct peaks, one peak located at ca. 529.0 eV-530.0 eV corresponding to lattice oxygen (O_α) and two more at ca. 530.5-531.5 eV and 532.0-533.0 eV which can be attributed to surface adsorbed oxygen (O_β), such as chemisorbed oxygen, whereas the other oxygen species (O_γ, 533.2-535.0 eV and 534.8-535.6 eV) were associated with water and carbonate species (Long et al. 2019; Wang et al. 2018; Yang et al. 2020). The surface absorbed oxygen content of the catalysts is calculated in Table 2. It is apparent that the introduction of Mn promoted higher relative O_{ads} concentration, which could enhance the oxidation reaction process. After the addition of Fe, Co, Sn, the percentage of O_{ads} content evidently decreased.

Reducibility

Figure 4 presented H$_2$-TPR results of the catalysts. The H$_2$-TPR profiles showed three peaks between 50 and 700 °C. For the pure MnO$_x$ catalyst, three peaks located around 178 °C,
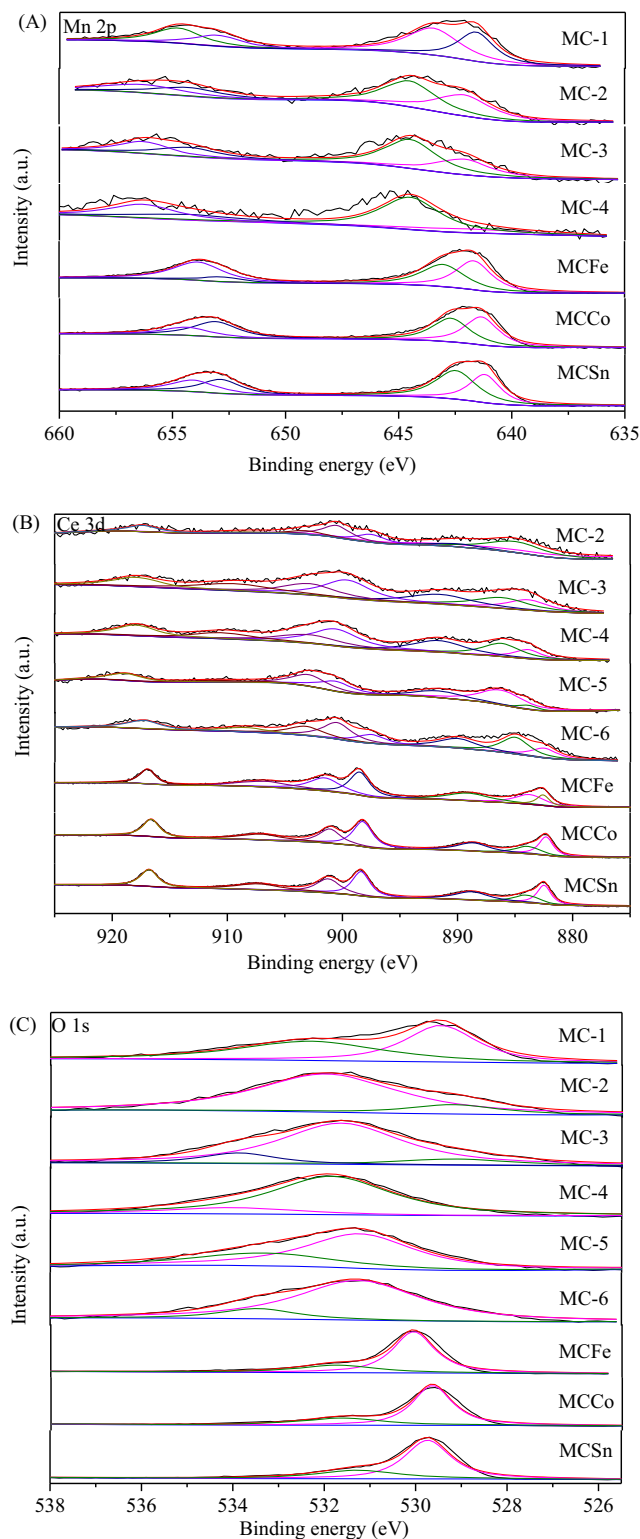

Fig. 3. A Mn 2p, B Ce 3d, C O 1s XPS spectra of different samples.

310 °C, and 428 °C in the curve of MnO$_x$, which were related to the reduction of MnO$_2$/Mn$_2$O$_3$→Mn$_3$O$_4$→MnO (Lin et al. 2018). For the pure CeO$_x$ catalyst, the main reduction peaks were detected at 491 °C and 693 °C , the 491 °C peak can be

Table 2 Surface element relative percentage of the Mn-Ce catalysts

Catalysts	Mn 2p (eV)		Mn distribution (%)		Ce distribution (%)		$O_\beta/(O_\alpha+O_\beta+O_\gamma)$ (%)
	Mn^{3+}	Mn^{4+}	Mn^{3+}	Mn^{4+}	Ce^{3+}	Ce^{4+}	
MC-1	641.6	643.5	42.53	57.47	/	/	51.07
MC-2	642.1	644.5	45.94	54.06	/	/	86.12
MC-3	642.1	644.5	39.69	60.31	29.18	70.82	77.30
MC-4	642.0	644.5	27.46	72.54	29.66	70.34	85.10
MC-5	/	/	/	/	45.40	54.60	33.95
MC-6	/	/	/	/	36.71	63.29	13.29
MCFe	641.9	643.4	39.86	60.14	26.93	73.07	26.17
MCCo	641.35	642.76	56.27	43.73	21.57	78.43	28.04
MCSn	641.19	642.58	45.96	54.04	22.28	77.72	29.15

attributed to the Ce^{4+} reduced to Ce^{3+}, while the 693°C peak was due to the same process in catalysts. The metal Ce doping resulted in the first H$_2$ reduction peak shift to a higher temperature. The Mn-Ce oxide (MC-2, MC-3, MC-4) catalysts showed similar reduction peaks at 250 °C, 310 °C, and 420 °C, respectively. For the MCFe and MCCo catalyst, the main reduction peaks were detected at 252.3°C and 396.6 °C, 218.8 °C and 394.5 °C, respectively. The MCSn catalyst showed three reduction peaks at 269.6 °C, 410.4 °C, and 544.9 °C. The reduction peak below 400 °C were ascribed to the Mn^{4+}/Mn^{3+} (Mn^{2+}) reduction; the reduction peak above 400 °C were related to the Ce^{4+} reduced to Ce^{3+} (Lin et al. 2018).

The H$_2$ consumption for each catalyst is calculated in Table 3. Compared with MC-2, it is evident that the H$_2$ consumption of peak at 269.6 °C, 410.4 °C, 252.3 °C,

and 396.6 °C for MCSn and MCFe was much higher than that of the other catalysts. The increase of H$_2$ consumption means the formation of more oxygen vacancies, which facilitates the oxygen mobility and enhances the active catalytic reaction. After Fe, Co, and Sn doping, the low-temperature oxidation of the catalyst was enhanced, which was significantly stronger than that of the single-component catalyst.

Catalytic performance

Catalytic activity

Figure 5 shows the 1,2-DCB oxidation catalytic performance of the catalysts. Among all the catalysts, CeOx has the lowest catalytic removal efficiency. The increase of Mn significantly increased the 1,2-DCB conversion efficiency. MC-2 showed better activity at lower temperatures (150–180 °C), the removal efficiency of 1,2-DCB was 64.72 % at 180 °C. At 360 °C, the removal efficiency of 1,2-DCB was 88.86 %. The addition of Fe, Co, Sn in MC-2 did not improve the oxidation efficiency. Table 4 illustrates the 1,2-DCB oxidation activities of Mn-based oxides in literatures. It was found that the performance results are consistent with the results of O1s in XPS and H$_2$-TPR. Compared with other catalysts, the MC-2 sample contains more adsorbed oxygen and redox sites. Generally, structures, morphologies, and redox properties were the main factors determining the catalytic activity of metal oxides (Chen et al. 2018).

Selectivity

Carbon dioxide (CO$_2$), carbon monoxide (CO), H$_2$O, hydrogen chloride (HCl), and chlorine (Cl$_2$) were the major inorganic products obtained in the 1,2-DCB catalytic oxidation process Li et al. 2021). CO$_2$, CO, and HCl selectivity represents the important performance of a catalyst for catalytic oxidation of 1,2-DCB (Lin et al. 2021; Deng et al. 2018). As
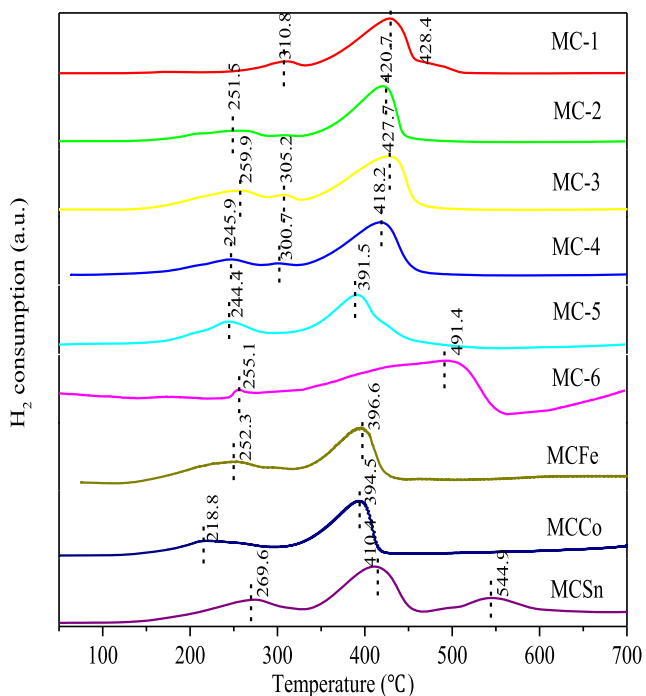

Fig. 4. H$_2$-TPR profiles of the Mn-Ce catalysts

Table 3 Redox properties of the Mn-Ce catalysts.

Sample	H$_2$ consumption (mmol H$_2$/g)						Experimental H$_2$ consumption of catalyst (mmol H$_2$/g)
	Position (°C)	Peak 1	Position (°C)	Peak 2	Position (°C)	Peak 3	
MC-1	178.8	0.041	310.8	0.36	428.4	2.92	3.32
MC-2	251.5	0.59	307.1	0.12	420.7	2.42	3.13
MC-3	259.9	0.57	305.2	0.15	427.7	1.71	2.43
MC-4	245.9	0.27	300.7	0.10	418.2	1.15	1.52
MC-5	244.4	0.37	391.5	0.85	/	/	1.21
MC-6	255.1	0.0041	491.4	0.20	693.2	0.059	0.32
MCFe	252.3	3.38	396.6	5.51	/	/	8.89
MCCo	218.8	1.07	394.5	1.99	/	/	3.06
MCSn	269.6	3.82	410.4	7.98	544.9	3.79	15.59

Table 4 Main data of research papers on 1,2-DCB over the Mn-based oxides catalysts

Catalysts	Preparation method	Pollutants	Reaction condition	Conversion (at 240°C)	Refs.
MnCeOx	Wet chemical method	1,2-DCB	400–600 ppm 120 ml/min air WHSV 12000 h^{-1}	73 %	Tang et al. 2016
MnCoOx	Co-precipitation	1,2-DCB	1000ppm 10% O$_2$ WHSV 15000 h^{-1}	10 %	Cai et al. 2015
MnCeOx MnCeOx	Co-precipitation Impregnation	1,2-DCB+NO+ NH$_3$	1,2-DCB 100 ppm NO 300 ppm NH$_3$ 300 ppm 10% O$_2$ WHSV 40000 h^{-1}	85 % 30 %	Martín-Martín et al. 2020
MnCeOx	Co-precipitation	1,2-DCB	108 ppm 10% O$_2$ WHSV 12000 h^{-1}	79 %	This Paper

shown in Fig. 6, the dominant products in the effluent gas over MC-1, MC-2, MC-3 and MCFe, MCCo, and MCSn catalysts showed a change in trend in the temperature range of 150–360°C. The yields of CO and CO$_2$ obtained below 240 °C gradually increased with the increase of temperature, whereas the yields of CO and CO$_2$ increased quickly up to their maximum values by 330°C. For MC-3, CO$_2$ production increased rapidly up to their maximum values at 330°C and then decreased slowly. In comparison with the MC-2 catalyst, the selectivity of CO$_2$/CO increased after the addition of Fe, Co, and Sn. At 270°C, the selectivity of MCFe towards CO$_2$ and CO reached 96% and that of MCCo was 93% and 100% at 330°C and 360°C, respectively. The higher selectivity of CO$_2$/ CO might be attributed to the addition of Fe.

As shown in Fig. 7, HCl in the effluent gas over catalysts shows a similar change in trend in the temperature range of 120–360°C, the concentration of HCl were low below 330°C, whereas the concentration of HCl increased quickly at 360°C. The HCl concentration in tail gas of catalytic oxidation over

MCFe was higher than other catalysts. For other organic byproducts, C$_3$H$_6$O$_2$ was the first organic byproduct to be
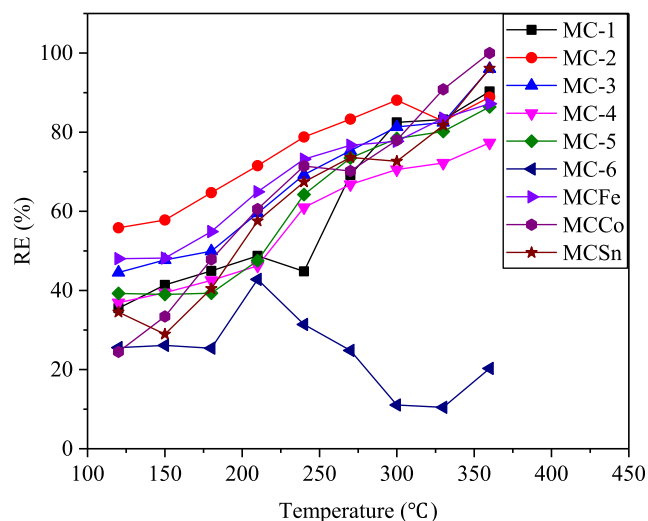
Fig. 5. Catalytic performance of the Mn-Ce catalysts
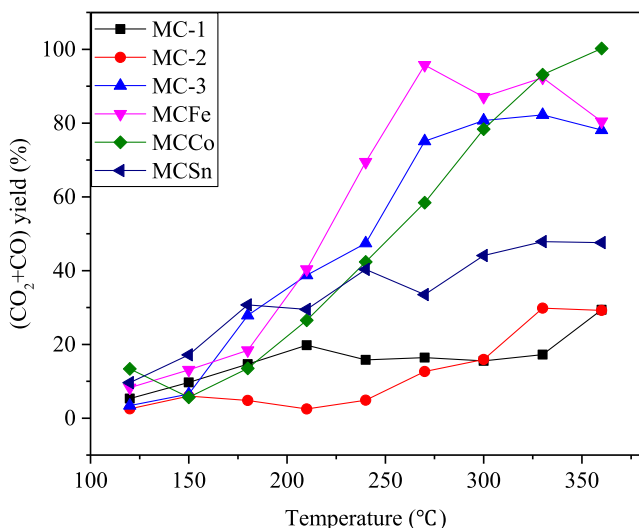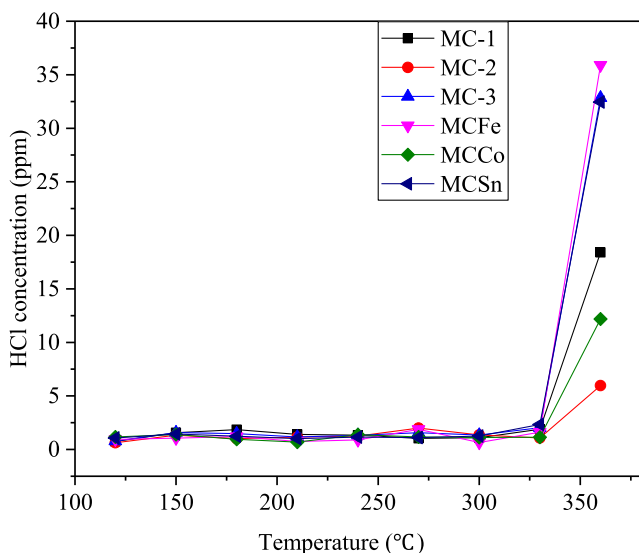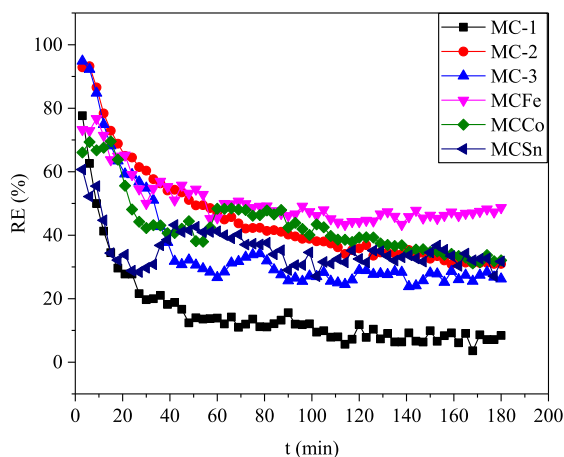
Fig. 6. The CO_2/CO yield over catalysts

Fig. 7. The HCl yield over catalysts

identified, and the second organic byproduct was CB. For other byproducts, the amounts were relatively stable and small, and the order of production was $C_3H_6O_2$, C_6H_5Cl, CH_4O, CH_4, CH_2O_2.

Stability of the catalysts

Deactivation is an important aspect in the catalytic oxidation of 1,2-DCB. The stability of MC-1, MC-2, MC-3 and MCFe, MCCo, MCSn for 1,2-DCB catalytic oxidation was evaluated at 180 °C and 300 °C. The results are shown in Fig. 8. The pure MnOx catalyst (MC-1) has the lowest stability. Compared with MC-1, the addition of CeOx could promote resistance to Cl poisoning. Previous researches have shown that the strong adsorption of chlorine species (Cl2, HCl, etc.) would block active sites (Long et al. 2019). As shown in Fig. 8, MC-2 has better stability than other MC catalysts at 180 °C. Within 180 min, the removal efficiency is stable at about 40 %. After the addition of Fe, Co, Sn, the stability of catalysts could be promoted, and MCFe exhibited better stability at 180 °C. And after 180 min, the removal efficiency was about 50 %. However, the stability improved significantly at higher temperature. MCCo and MCSn exhibited better stability at 300 °C, and after 300 min, the removal efficiency was about 65 %.

Products and mechanism

The oxidation of 1,2-DCB was carried out on the catalyst MC-3 at 330°C. The effluent gas after the reaction was adsorbed on an adsorption tube (Tenax) for 30 min. The byproducts in the adsorption tube were desorbed by thermal analysis and a desorption device and then entered into GC-MS for analysis. As shown in Fig. 9 and Table 5, the main byproducts in the 1,2-DCB oxidation process contain CO_2 (16.58 %), C_3H_8 (4.25 %), C_3H_6O (4.87 %), C_4H_8O (4.92 %), $CHCl_3$ (8.85 %), CCl_4 (25.75 %), C_6H_6 (1.61 %), C_2HCl_3 (1.96 %), $C_5H_{10}O$ (2.41 %), $C_3H_6O_2$ (1.06 %), C_7H_8 (6.27 %), $C_6H_{12}O$ (1.63 %), C_6H_5Cl (1.07 %),
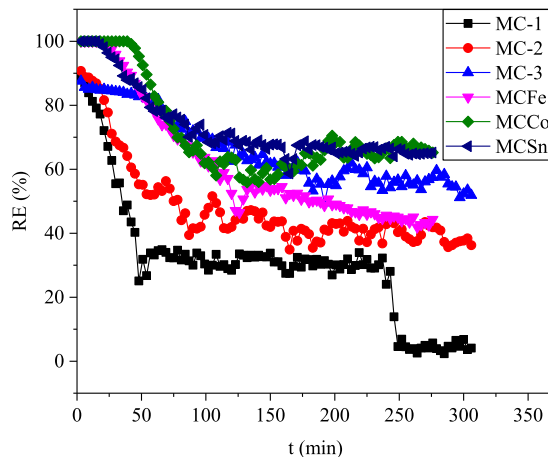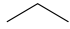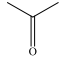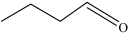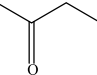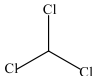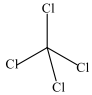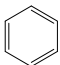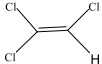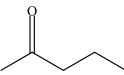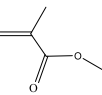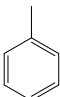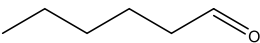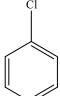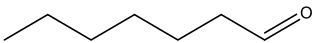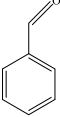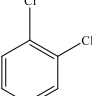

Fig. 8. Stability test of catalysts at **A** 180 °C and **B** 300 °C

Table 5 Intermediate products of 1,2-DCB on MC-3 catalyst

Label	Molecular formula	Name of compound	Molecular structure	Percentage (%)
1	CO_2	Carbon dioxide	CO_2	16.58
2	C_3H_8	Propane		4.25
3	C_3H_6O	Acetone		4.87
4	C_4H_8O	Butanal		1.84
	C_4H_8O	2-Butanone		3.08
5	$CHCl_3$	Trichloromethane		8.85
6	CCl_4	Carbon Tetrachloride		25.75
7	C_6H_6	Benzene		1.61
8	C_2HCl_3	Trichloroethylene		1.96
9	$C_5H_{10}O$	2-Pentanone		1.00
	$C_5H_{10}O$	Pentanal		1.41
10	$C_3H_6O_2$	2-Propenoic acid		1.06
11	C_7H_8	Toluene		6.27
12	$C_6H_{12}O$	Hexanal		1.63
13	C_6H_5Cl	Chlorobenzene		1.07
14	$C_7H_{14}O$	Heptanal		1.12
15	$C_{10}H_{12}$	Decane		1.79
16	C_6H_5CHO	Benzaldehyde		1.80
17	$C_6H_4Cl_2$	1,2-dichlorobenzene		14.07
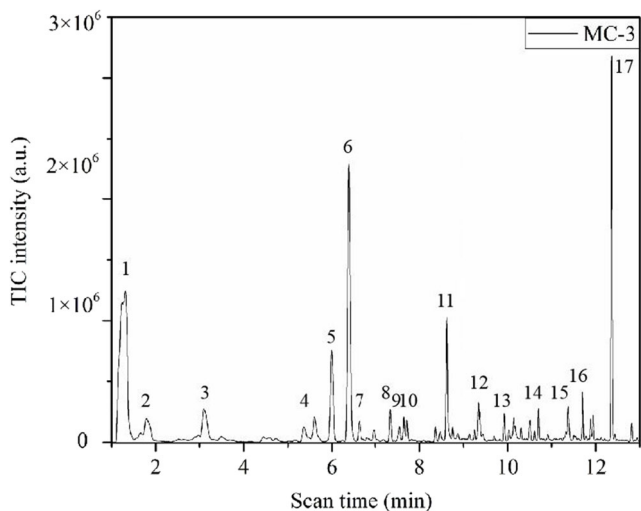
Fig. 9. GC-MS analyses on the intermediate products for MC-3 catalyst.

$C_7H_{14}O$ (1.12 %), $C_{10}H_{12}$ (1.79 %), C_6H_5CHO (1.80 %) (labels 1–16 in Table 5), and $C_6H_4Cl_2$ (14.07 %) (label 17 in Table 5). As shown in Table 5, the MC-3 catalyst produced approximately four kinds of chlorinated organics (labels 5, 6, 8, and 13 in Table 5) and 11 kinds of non-chlorinated chain organics (labels 2, 3, 4, 7, 9, 10, 11,12, 14, 15, and 16). In particular, the CB and 1,2-DCB byproducts were detected in the effluent gas.

The reaction paths were proposed based on the byproducts detected by GC/MS and Gasmet FT-IR gas analyzer. The oxidation route of 1,2-DCB over MnCeOx is shown in Fig. 10. The 1, 2-DCB was first absorbed on the Lewis sites of the MnCeOx catalyst, and then the C–Cl bond was abstracted by

nucleophilic substitution of the oxygen from OH groups and the formation of the chlorophenoxy species (i). The Cl of the phenolate species reacted with the OH of the catalyst to form catecholates species, which are transmuted into benzoquinone species (ii). At this stage, the C-Cl bond was weaker than C-H band for aryl halides. There are two pathways for the dechlorination reaction for 1,2-DCB: elimination of a HCl molecule and elimination of two HCl molecules (Li et al. 2021; Long et al. 2019; Lei et al. 2021; Wang et al. 2020). And the C-Cl bond in CB broke first and formed phenyl radical and chlorine iron, phenyl radical is attacked by hydroxyl radical and transformed to phenoxy radical, and then reacts with active oxygen species to generate oxygenated hydrocarbons, and then decomposes to aldehydes or ketones (Long et al. 2019). The carbon of the (i) and (ii) species were attacked by active oxygen species via nucleophilic substitution reactions, resulting in the fracture of the carbon-carbon bonds, then oxidized into acetate or maleate species (Li et al. 2021; Cai et al. 2015; He et al. 2015; Sun et al. 2016b). A fragment of 1,2-DCB was oxidized to chlorinated hydrocarbons via electrophilic substitution (Long et al. 2019). These byproducts could undergo further oxidization to the final products, namely, CO_2, H_2O, HCl, and so on.

Conclusion

In this work, Mn and Ce oxides were prepared by co-precipitation, and the physicochemical properties of the as-prepared
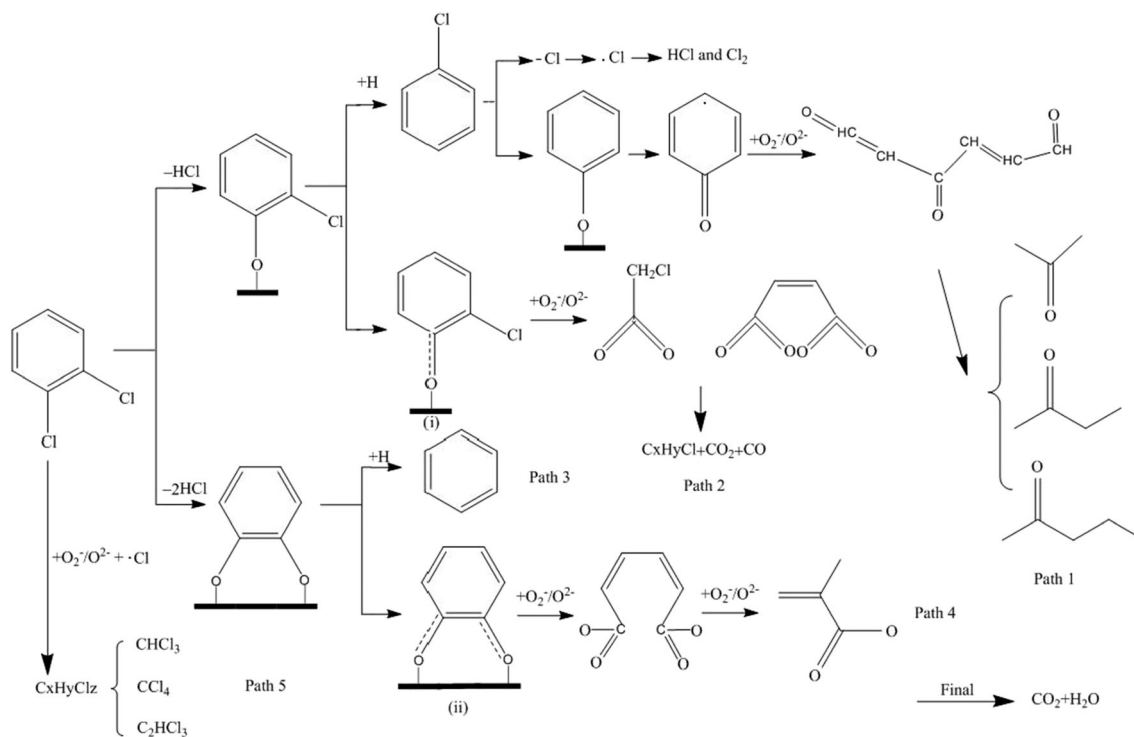

Fig. 10. Proposed oxidation pathway of 1,2-DCB over Mn-Ce catalysts

catalysts were studied. The catalytic activity, selectivity, and stability of catalysts on 1,2-DCB oxidation were tested. Doping Ce to the MnO_x structure in co-precipitated catalysts enhances the redox properties and catalytic oxidation efficiency. Stability tests were used to evaluate the deactivation rate in all catalysts, and better stability could be seen in MCFe at low temperatures and in MCSn at higher temperatures. CO_2, CO products in the effluent gas were analyzed on line, the selectivity of MCFe towards CO_2 and CO reached 96% at 270 °C. Intermediate products of the 1,2-DCB oxidation process over MC-3 were analyzed by GC-MS, and the effluent gas was analyzed using a Gasmet FT-IR gas analyzer. Finally, the reaction paths were proposed.

Declarations

Ethics approval and consent to participate Not applicable

Consent for publication Not applicable

Competing interests The authors declare no competing interests.

References

Cai T, Huang H, Deng W, Dai QG, Liu W, WangXY (2015) Catalytic combustion of 1,2-dichlorobenzene at low temperature over Mn-modified Co_3O_4 catalysts. Appl Catal B Environ:166–167-393-405

Chen J, Chen X, Xu WJ, Xu Z, Jia HP, Chen J (2018) Homogeneous introduction of CeOy into MnOx-based catalyst for oxidation of aromatic VOCs. Appl Catal B Environ 224:825–835

Debecker DP, Bertinchamps F, Blangenois N, Eloy P, Gaigneaux EM (2007) On the impact of the choice of model VOC in the evaluation of V-based catalysts for the total oxidation of dioxins: furan vs. chlorobenzene. Appl Catal B Environ 74:223–232

Deng L, Ding YP, Duan BQ, Chen YW, Li PW, Zhu SM, Shen SB (2018) Catalytic deep combustion characteristics of benzene over cobalt doped Mn-Ce solid solution catalysts at lower temperatures. Mol Catal 446:72–80

Deng W, Tang QX, Huang SS, Zhang L, Jia ZY, Guo LM (2020) Low temperature catalytic combustion of chlorobenzene over cobalt based mixed oxides derived from layered double hydroxides. Appl Catal B Environ 278:119336

He C, Yu YK, Shi JW, Shen Q, Chen JS, Liu HX (2015) Mesostructured Cu-Mn-Ce-O composites with homogeneous bulk composition for chlorobenzene removal:Catalytic performance and microactivation course. Mater Chem Phys 157:87–100

Lei M, Tang Y, Wang HM, Zhu LH, Zhang GH, Yu Zhou Y, Tang HQ (2021) A catalytic strategy for rapid cleavage of C-Cl bond under mild conditions: Effects of active hydrogen induced by Pd nanoparticles on the complete dechlorination of chlorobenzenes. Chem Eng J 419:129510

Li N, Xing X, Cheng J, Zhang ZS, Hao ZP (2021) Influence of oxygen and water content on the formation of polychlorinated organic by-products from catalytic degradation of 1,2-dichlorobenzene over a Pd/ZSM-5 catalyst. J Hazard Mater 403:123952

Lin XT, Li SJ, He H, Wu Z, Wu JL, Chen LM, Ye DQ, Fu ML (2018) Evolution of oxygen vacancies in MnOx-CeO2 mixed oxides for soot oxidation. Appl Catal B Environ 223:91–102

Lin FW, Zhang ZM, Li N, Yan BB, He C, Hao ZP, Chen GY (2021) How to achieve complete elimination of Cl-VOCs: a critical review on byproducts formation and inhibition strategies during catalytic oxidation. Chem Eng J 404:126534

Liu H, Xian L, Dai QG, Zhao HL, Chai GT, Guo YL, Guo Y, Wang L, Zhan WC (2021) Catalytic oxidation of chlorinated volatile organic compounds over Mn-Ti composite oxides catalysts: elucidating the influence of surface acidity. Appl Catal B Environ 282:119577

Long GY, Chen MX, Li YJ, Ding JF, Sun RZ, Zhou YF, Huang XY, Han GR, Zhao WR (2019) One-pot synthesis of monolithic Mn-Ce-Zr ternary mixed oxides catalyst for the catalytic combustion of chlorobenzene. Chem Eng J 360:964–973

Martín-Martín JA, Sánchez-Robles J, González-Marcos MP, Aranzabal A, González - Velasco JR (2020) Effect of preparation procedure and composition of catalysts based on Mn and Ce oxides in the simultaneous removal of NOX and o-DCB. Mol Catal 495:111152

Venkataswamy P, Rao KN, Jampaiah D, Reddy BM (2015) Nanostructured manganese doped ceria solid solutions for CO oxidation at lower temperatures. Appl Catal B Environ 162:122–132

Shao JM, Lin FW, Li Y, Tang HR, Wang ZH, Liu PX, Chen GY (2019) Co-precipitation Synthesized MnOx-CeO2 Mixed oxides for NO oxidation and enhanced resistance to low concentration of SO_2 by metal addition. Catalysts 9:519

Ssebugere P, Sillanpää M, Matovu H, Mubiru E (2019) Human and environmental exposure to PCDD/Fs and dioxin-like PCBs in Africa: A review. Chemosphere 223:483–493

Sun YY, Zhong SF, Xin HC, Zhang F, Chen L, Li XB (2016a) Enhancement in oxidative property on amorphous rare earth doped Mn catalysts.Catal. Commun 77:94–97

Sun PF, Wang WL, Dai XX, Weng XL, Wu ZB (2016b) Mechanism study on catalytic oxidation of chlorobenzene over $Mn_xCe_{1-x}O_2$/H-ZSM5 catalysts under dry and humid conditions. Appl Catal B Environ 198:389–397

Sun PF, Wang WL, Weng XL, Dai XX, Wu ZB (2018) Alkali potassium induced HCl/CO2 selectivity enhancement and chlorination reaction inhibition for catalytic oxidation of chloroaromatics. Environ Sci Technol 52:6438–6447

Tang XF, Li YG, Huang XM, Xu YD, Zhu HQ, Wang JG, Shen WJ (2006) MnOx–CeO2 mixed oxide catalysts for complete oxidation of formaldehyde: Effect of preparation method and calcination temperature. Appl Catal B Environ 62:265–273

Tang AD, Hu LQ, Yang XH, Jia YR, Zhang Y (2016) Promoting effect of the addition of Ce and Fe on manganese oxide catalyst for 1,2-dichlorobenzene catalytic combustion. Catal Commun 82:41–45

Wang XY, Kang Q, Li D (2009) Catalytic combustion of chlorobenzene over MnOx–CeO2 mixed oxide catalysts. Appl Catal B Environ 86: 166–175

Wang Y, Deng W, Wang YF, Guo LM, Ishihara T (2018) A comparative study of the catalytic oxidation of chlorobenzene and toluene over Ce-Mn oxides. Mol Catal 459:61–70

Wang H, Peng B, Zhang RD, Chen HX, Wei Y (2020) Synergies of Mn oxidative ability and ZSM-5 acidity for 1, 2-dichloroethane catalytic elimination. Appl Catal B Environ 276:118922

Yang J, Ren S, Zhang TS, Su ZH, Long HM, Kong M, Lu Y (2020) Iron doped effects on active sites formation over activated carbon supported Mn-Ce oxide catalysts for low-temperature SCR of NO. Chem Eng J 379:122398

Zhang XJ, Zhao JG, Song ZX, Liu W, Zhao H, Zhao M, Xing Y, Ma ZA, Du HX (2020) The catalytic oxidation performance of toluene over the Ce-Mn-Ox catalysts: Effect of synthetic routes. J Colloid Interface Sci 562:170–181

Zhao J, Xi WJ, Tu CS, Dai QG, Wang XY (2020a) Catalytic oxidation of chlorinated VOCs over Ru/TixSn1-x catalysts. Appl Catal B Environ 263:118237

Zhao H, Li HC, Pan ZF, Feng F, Gu YW, Du JC (2020b) Design of CeMnCu ternary mixed oxides as soot combustion catalysts based on optimized Ce/Mn and Mn/Cu ratios in binary mixed oxides. Appl Catal B Environ 268:118422